Electronic Supplementary Material (ESI) for Nanoscale.

Supporting Information

Fluorescent and Magnetic Anti-Counterfeiting Realized by Biocompatible Multifunctional Silicon Nanoshuttles-Based Security Ink

*Bin Song, Houyu Wang, Yiling Zhong, Binbin Chu, Yuanyuan Su and Yao He**

Jiangsu Key Laboratory for Carbon-Based Functional Materials and Devices, Institute of Functional Nano & Soft Materials (FUNSOM) and Collaborative Innovation Center of Suzhou Nano Science and Technology (NANO-CIC), Soochow University, Suzhou 215123, China

E-mail: yaohe@suda.edu.cn

1. Experimental Procedures

1.1 Materials and devices

The (3-aminopropyl) trimethoxysilane (97%) was purchased from Sigma-Aldrich. Trisodium citrate dihydrate (≥ 99.0%) and ferric chloride (≥ 97.0%) were purchased from Sinopharm Chemical Reagent Co., Ltd (China). CdSe/ZnS quantum dots (QDs) were purchased from Wuhan Jiayuan Co., Ltd (China). Rhodamine 6G (R6G), Magnevist and Feridex were purchased from Sigma-Aldrich. All chemicals were used without additional purification. All solutions were prepared using Milli-Q water (Millipore) as the solvent. The microwave system NOVA used for synthesizing materials was made by Preekem of Shanghai, China. The system operated at 2450 MHz frequency and worked at 500 W power. Exclusive vitreous vessels with a volume of 15 mL were equipped for the system to provide security during reaction demanding high temperature and pressure. Microwave-assisted synthetic strategies for the production of silicon nanostructures and C-dots have been well described in our previous reports.[1,2] Transmission electronic microscope (TEM) and high resolution TEM (HRTEM) samples were prepared by dispersing the sample onto carbon-coated copper grids with the excess solvent evaporated. The TEM and HRTEM overview images were recorded using Philips CM 200 electron microscope operated at 200 kV. High-resolution X-ray photoelectron spectroscopy (XPS) analyses were performed using a Kratos AXIS Ultra^{DLD} ultrahigh vacuum (UHV) surface analysis system, which consists of a fast entry air lock (base pressure < 1×10^{-8} Torr), a multiport carousel chamber (< 5×10^{-10} Torr), a deposition chamber (< 5×10^{-10} Torr), and an analysis chamber (< 3×10^{-10} Torr). A monochromatic Al Kα source (1486.6 eV) with a resolution of 0.1 eV was used to irradiate the samples. XPS samples were prepared by drop-casting SiNSs (~2 mg) onto aluminum substrates and degassing at 10^{-7} Torr for 15 hours prior to analysis. All XPS spectra were internally calibrated to the C 1s emission (284.8 eV). Our samples were digested in microwave digestion system (EXCEL, Preekem Scientific Instruments Co. Ltd, Shanghai, China). The solution was diluted with Milli-Q water and the Fe and Si contents were determined with inductively coupled plasma-mass spectrometry (ICP-MS (aurora M90)). For Fourier transform infrared spectroscopy (FTIR) measurements, KBr was pressed into a slice, onto which the SiNSs sample was dropped. The solvent in the sample was adequately evaporated by irradiation (> 30 min) with a high-power incandescent lamp. FTIR

spectra were recorded on a Bruker HYPERION FTIR spectrometer and cumulated 32 scans at a resolution of 4 cm^{-1}. Energy-dispersive X-ray (EDX) spectroscopy was utilized to determine the fraction of the resultant materials. UV-vis absorption spectra were recorded with a Perkin Elmer Lambda 750 UV-vis-near-infrared spectrophotometer. Photoluminescence (PL) measurements were performed using a HORIBA JOBIN YVON FLUOROMAX-4 spectrofluorimeter. A Maestro in vivo optical imaging system (Cambridge Research & instrumentation, Inc.) was utilized for imaging our samples. A Laser-scanning confocal fluorescent (Leica, TCS-SP5) (LSCM), equipped with diode laser (405 nm) and argon laser (458, 476, 488 and 514 nm), was used for fluorescent imaging. Images were captured and processed with image analysis software. Our samples were scanned under a 3 T clinical MRI scanner (Bruker Biospin Corporation, Billerica, MA, USA) at room temperature. The amounts of SiNSs in the aqueous solution were manually tuned to realize the T_1 and T_2 - weighted MR images. After acquiring the T_1-and T_2-weighted MR images, the intensities of images were measured within manually drawn regions of interest for each sample.

1.2 Synthesis of silicon nanoshuttles (SiNSs), silicon nanoparticles (SiNPs) and carbon dots (C-dots)

In our experiment, the precursor solution was prepared by adding 2 ml of (3-aminopropyl) trimethoxysilane to 8 ml N_2-satureted aqueous solution dispersed with 0.075 g of trisodium citrate. Then, 0.05 mmol iron (III) chloride was mixed into the citric acid aqueous solution under constant stirring. The mixture was stirred for 30 min. The resultant precursor solution was transferred into the exclusive vitreous vessel with a volume of 15 ml. The SiNSs were prepared under 150 ^oC/30 min. To exclude impurities influence, such as (3-aminopropyl) trimethoxysilane molecules, trisodium citrate and iron (III) chloride in solution, the residual reagents were removed by dialysis (500 Da). The samples of SiNSs were separated through centrifugation at 5000 rpm for 10 min to achieve the pure SiNSs free of impurity. The purified SiNSs were then concentrated to an applicable concentration for following characterizations and applications.[1a]

For the preparation of SiNPs, the SiNPs precursor solution was prepared by adding 1 mL (3-aminopropyl) trimethoxysilane to 8 mL N_2-saturated aqueous solution dispersed with 0.075 g trisodium citrate dihydrate. The mixture was stirred for 10 min.

The resultant precursor solution was transferred into the exclusive vitreous vessel with a volume of 30 mL. The SiNPs were prepared under 150 °C/60 min. To exclude impurities influence, the residual reagents were removed by dialysis (500 Da). The purified SiNPs aqueous solution was used for characterizations and applications. For the fabrication of C-dots, 20 mL milk was first put into the vessel and heated to 175 °C for 25 min. When cooled down to room temperature, the obtained solid was dialyzed using pure water through a dialysis membrane (500 Da). The purified C-dots were finally collected for photostability comparison.[1b,c]

1.3 Photoluminescent quantum yields (PLQY) measurements

In our experiment, a well-established method was employed for determining the PLQY value of SiNSs as follow (Quinine sulfate in 0.1 M H_2SO_4 (literature quantum yield: 58%)).[1]

$\Phi_x=\Phi_{st}\,(I_x/I_{st})\,(\eta_x/\eta_{st})^2\,(A_{st}/A_x)$

Where Φ is the QY, "I" is the integrated emission intensity, "η" is the refractive index of the solvent, and A is the optical density. The subscript "st" and "x" stand for standard with known QY and the SiNSs sample, respectively. The resultant SiNSs feature relatively strong fluorescence with a PLQY of ~19%.

1.4 Photostability of SiNSs

The photoluminescence intensity of R6G, CdSe/ZnS QDs, C-dots and SiNSs were adjusted to the same value. The three samples were continuously irradiated for different time intervals using a lamp of 365 nm. The images were captured by digital single lens reflex.

1.5 Multicolor imaging and anti-counterfeiting

Typically, a Maestro in vivo optical imaging system (Cambridge Research & instrumentation, Inc.) was utilized for imaging the solution samples of SiNSs (2 mg/mL), SiNPs (2 mg/mL) and R6G (0.2 mg/mL). In particular, excitation wavelength: 365 nm, blue emission window: 465-490 nm, exposure time: 1000 ms; excitation wavelength: 455 nm, green emission window: 490-530 nm, exposure time: 1000 ms; excitation wavelength: 523 nm, yellow emission window: 550-590 nm, exposure time: 1000 ms.

The cartridge of an inkjet printer was filled with the prepared SiNSs (2 mg/mL), SiNPs (2 mg/mL) and R6G (0.2 mg/mL). A common printer was used for printing the desired numbers onto a piece of paper. A Maestro in vivo optical imaging system (Cambridge Research & instrumentation, Inc.) was utilized for imaging the stained papers (excitation wavelength: 365 nm, blue emission window: 465-490 nm, exposure time: 1000 ms; excitation wavelength: 455 nm, emission green window: 490-530 nm, exposure time: 1000 ms; excitation wavelength: 523 nm, yellow emission window: 550-590 nm, exposure time: 1000 ms).

Dacron fibers were doused in SiNSs ink. SiNSs ink was drop-casted on the hydrophilic photolithography design for patterning micro-scale structures. Dacron fibers and photo-lithography silicon wafer were mounted on slides in fluoromount (Sigma, F4680) with coverslips. Samples, which were examined under a confocal laser microscope (Leica, TCS-SP5) equipped with laser 405 nm (emission at 430-480 nm), 458 nm (emission at 470-550 nm) and 514 nm (emission at 560-620 nm). The leaf veins were coated with a drop of the aqueous solution of SiNSs ink and R6G respectively and then dried under air. The leaf veins were continuously irradiated for different time intervals using a lamp of 365 nm. A Maestro in vivo optical imaging system (Cambridge Research & instrumentation, Inc.) was utilized for imaging leaf veins (excitation wavelength: 365 nm, emission window: 465-490 nm, exposure time: 1000 ms; excitation wavelength: 455 nm, emission window: 490-530 nm, exposure time: 1000 ms; excitation wavelength: 523 nm, emission window: 550-590 nm, exposure time: 1000 ms).

The desired words or numbers were printed onto papers by a common commercial stamper using SiNSs ink. Different kinds of banknotes were chosen as printed paper which was proved as a suitable substrate for the SiNSs to adhere to and featured multi-color fluorescence. The banknotes were printed by stamper using SiNSs ink concentration of 2 mg/mL, then dried under air for application. Therefore, the designed words “Si silicon” and numbers “28.086” with multi-emission can be detected in banknotes under different irradiation. The images were captured by digital single lens reflex, under 365 nm, 400 nm and 450 nm irradiation, respectively.

1.6 Magnetic anti-counterfeiting

In the well plates, contrast agent (Magnevist, Feridex and SiNSs) were filled in each

of the wells according to the designed sequence with concentration of 0.1 mg/ml. T_1 and T_2 images of well plates filled with contrast agent were post processed through MRI imaging. MRI imaging of well plates were performed by using a 3.0 T MRI. T_1 images were determined using the following sequence: T_R = 625 ms, T_E = 10 ms, FOV = 75 mm, and acquisition number = 1. T_2 images were obtained by using the following fast spin echo sequence: T_R = 4000 ms, T_E = 80 ms, FOV = 75 mm and acquisition number = 1.

1.7 The MTT assay of cell viability

HeLa (Henrietta Lacks) cells (in H-DMEM medium) were dispersed in 96-well plates (100 μL in each well containing 1×10^4 cells per well). Serial concentrations (31.3, 62.5, 125, 250 and 500 μg/mL) of SiNSs solutions as that used in the following cellular imaging were added to each well (10 μL). Incubation was carried out for 0.5, 3, 6, 12, 24 and 48 h in a humidified atmosphere at 37 °C with 5% CO_2. The cytotoxicity of the SiNSs was evaluated by the MTT (3-(4, 5-dimethylthiazol-2-yl)-2, 5-diphenyltetrazolium bromide) assay (Thiazolyl blue tetrazolium bromide (M5655); Sigma). The assay was based on the accumulation of dark blue formazan crystals inside living cells after exposure to MTT, which is well-established for assessment of cellular viability. The destruction of cell membranes by the addition of sodium dodecylsulfate (SDS) resulted in the liberation and solubilization of the crystals. The number of viable cells was thus directly proportional to the level of the initial formazan product created. The formazan concentration was finally quantified using a spectrophotometer by measuring the absorbance at 570 nm (ELISA reader). A linear relationship between cell number and optical density was established, thus allowing an accurate quantification of changes in the rate of cell proliferation.

2. Additional data

Figure S1 shows EDX spectra and EDX mapping images of the SiNSs.

Figure S2 shows XPS spectra of the SiNSs.

Figure S3 shows FTIR spectra of the SiNSs.

Figure S4 shows fluorescence spectrum and corresponding normalized spectrum of the SiNSs under different excitation wavelengths.

Figure S5 shows PL decay curves of the prepared SiNSs.

Figure S6 shows plot of T_2^{-1} versus Fe concentration of SiNSs.

Figure S7 shows photostability comparison of R6G, CdSe/ZnS QDs, C-dots and SiNSs under continuous UV irradiation.

Figure S8 shows cell viability and morphology of HeLa cells treated with the SiNSs for different incubation time.

Figure S9 shows images of leaf veins stained with the SiNSs ink.

Figure S10 shows fluorescent images of synthetic fibers coated with the SiNSs ink.

Figure S11 shows hydrophilic photolithography patterns coated with the SiNSs ink.

Figure S12 shows optical and fluorescent images of the stamper stained with the SiNSs ink.

Figure S13 shows optical and fluorescent images of the stamper and synthetic fibers stained with the SiNSs ink before and after 30 day storage.

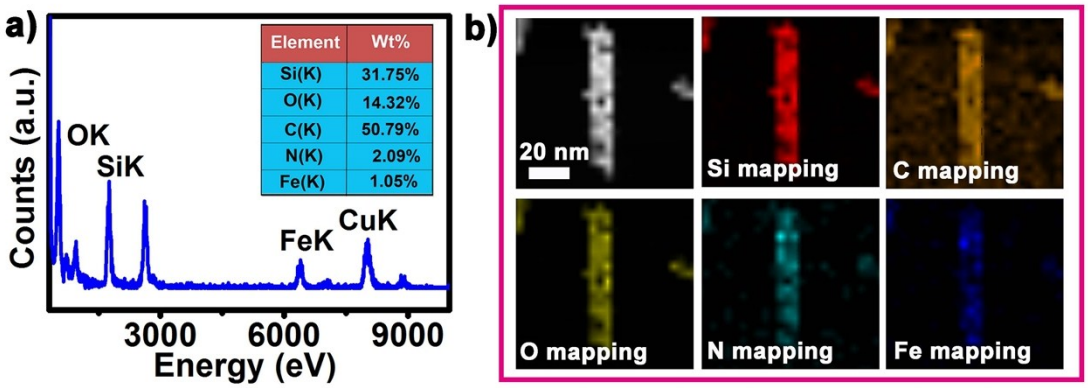

Figure S1. (a) EDX spectra and (b) EDX elemental maps of the prepared SiNSs.

To further analyze the chemical compositions of SiNSs, the EDX analyses reveals that the SiNSs contain Si, O, C, N and Fe of 31.75, 14.32, 50.79, 2.09 and 1.05 wt%, respectively. It is worthwhile to point out that, for EDX measurement, a quantitative analysis of the elemental ratios is not possible since the supporting substrate (e.g., carbon-coated copper girds) was carbon containing a measurable amount of residual oxygen. Therefore, the Si and Fe contain in EDX are lower than the results from ICP-MS. The EDX elemental maps of SiNSs confirm that the SiNSs contain Si, O, C, N and Fe elements, as indicated by red, orange, yellow, green and blue color, respectively.[2]

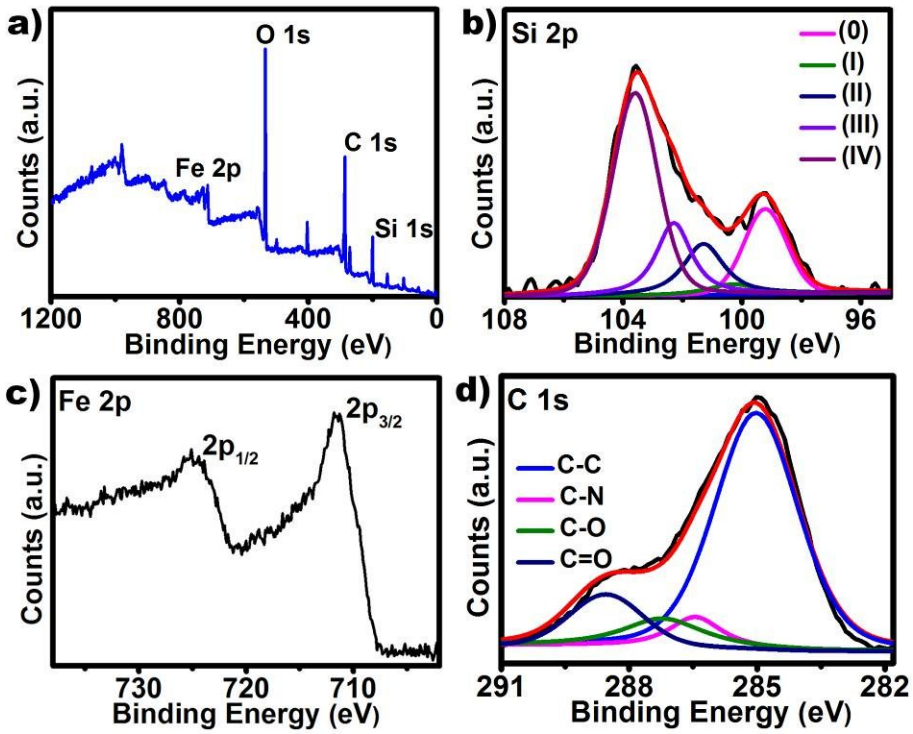

Figure S2. XPS spectra of the SiNSs with the assignment of characteristic peaks.

As shown in Figure S2 (a), four peaks at 103, 398, 286, 533 and 725 eV (ascribed to Si 2p, C 1s, N 1s, O 1s and Fe 2p) are observed, demonstrating the existence of Si, C, N, O and Fe elements in the SiNSs. Notably, high-resolution XPS of Si 2p region (Figure S2 (b)) shows an intense emission at 99.3 eV, which confirms the presence of Si (0). In addition, signals arising from Si surface atoms as well as Si suboxides are observed at 100.3, 101.3, 102.3, and 103.4 eV. For the Fe 2p spectrum, two peaks at 724.6 and 711.2 eV are observed, which are ascribed to the $2p_{1/2}$ and $2p_{3/2}$ (Figure S2 (c)), respectively. Therefore, we deduce that the valence state of iron element is Fe^{3+}.[1d] Figure S2 (d) presents the typical C 1s spectrum, exhibiting four distinct peaks located at 284.8, 285.3, 286.1, and 288.5 eV, which are ascribed to C-C, C-N, C-O and C=O, respectively.[1]

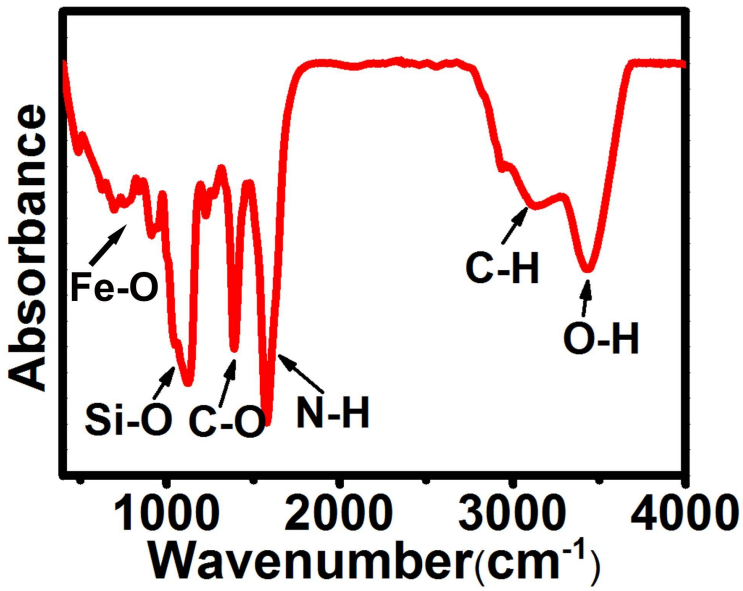

Figure S3. FTIR spectra of the SiNSs with the assignment of characteristic peaks.

The 3200-3700 cm^{-1} region is corresponding to the -OH stretching vibration. Sharp absorbance peaks at 1000-1200 cm^{-1} are attributed to the Si-O-Si asymmetric stretch vibrations. The 400-800 cm^{-1} region is ascribed to O-Si-O bending vibrations. The strong absorbance at 1390-1440 and 1580 cm^{-1} are, respectively, assigned to the C-O and N-H bending vibrations. The 800-900 cm^{-1} region is corresponding to asymmetric Fe-O stretching vibrations.[3c] The FTIR results demonstrate that the resultant SiNSs have a large amount of amino groups and carbon-related matrix.[3]

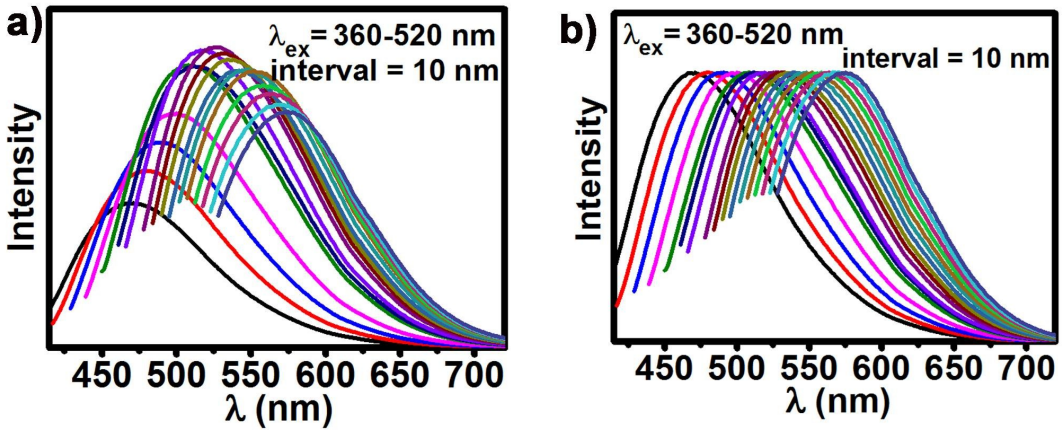

Figure S4. (a, b) Fluorescence spectra and corresponding normalized spectrum of the SiNSs under different excitation wavelengths.

As shown in Figure S4, the SiNSs yield selective emission peaks in a broad color range over the visible region ranging from ~450 nm to ~570 nm under serial excitation wavelengths from 360 to 520 nm. The Fe-related species on the surface of SiNSs may lead to the Fe impurity levels sited in the band gap of SiNSs, which induce the multilevel traps. Besides of this, according to the microwave-absorbing properties of Fe^{3+} ion species, local "hot surfaces" on SiNSs may be produced, bringing about the multiple structures in this synthesis.[4]

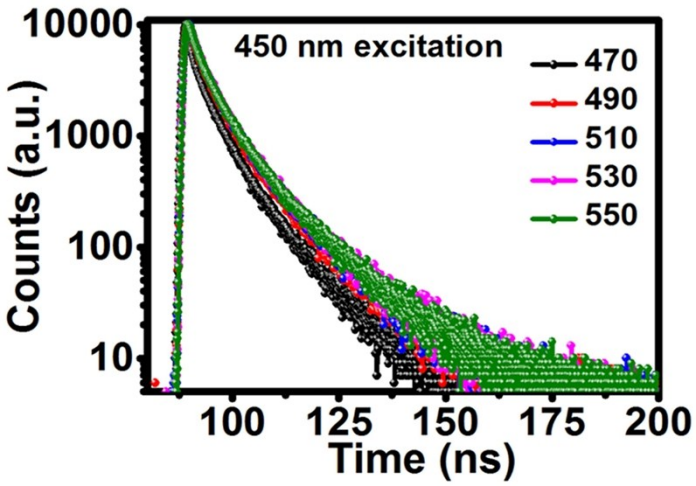

Figure S5. Time-resolved fluorescence-decay curves of SiNSs ($\lambda_{excitation}$ = 450 nm).

Typically, the fluorescence lifetime spectra of SiNSs (i.e., ~6.61 ns) are consistent with other time-scale (ns) of defect-related emission from silicon nanomaterials with strong blue fluorescence, suggesting the strong blue fluorescence of SiNSs is also from the exciton recombination at localized defect states, occurred at the surfaces of silicon nanomaterials. Here, multi-wavelength analyses indicate that the fluorescence decay is rather heterogeneous throughout the measured range. In particular, the luminescence tends to be longer lived in the blue region, that is, around 470 nm, than in the red, around 550 nm with average lifetimes of 6.61 and 3.21 ns, respectively. Furthermore, these measurements afford luminescence time profiles that are best fit by triexponential fitting functions. This suggests several kinds of emission centers within the SiNSs, providing valuable information for fluorophore efficiency improvement.[5]

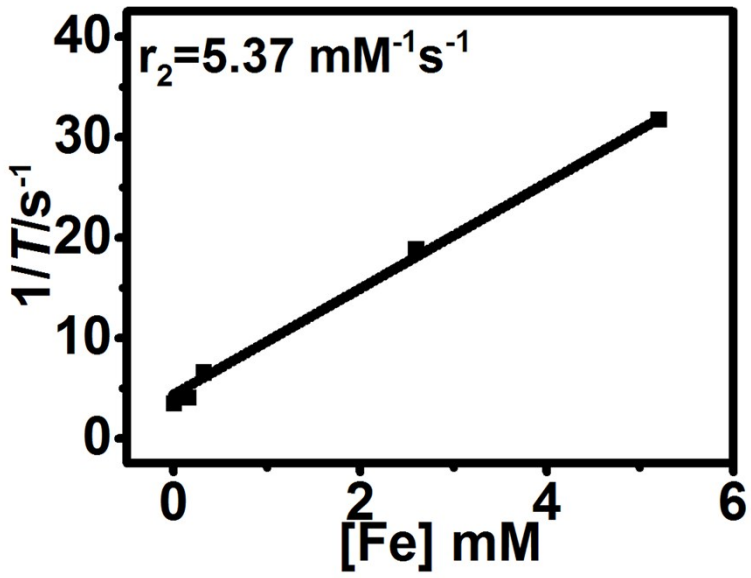

Figure S6. Plot of T_2^{-1} versus Fe concentration of SiNSs.

The magnetic responses of SiNSs are further tested by the relaxivity measurement, using a 3.0 T human clinical scanner. As revealed in Figure S6, The signal intensity increases significantly with the increase of Fe concentration (the samples have been concentrated to applicable concentrations), and the transverse relaxivity (r_2) value of the SiNSs are 5.37, which is consistent with our previous work.[1a]

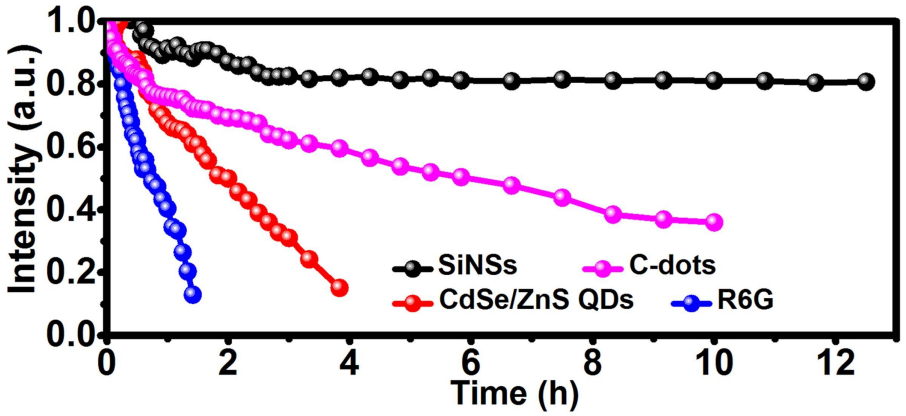

Figure S7. Photostability comparison of R6G, CdSe/ZnS QDs, C-dots and SiNSs under continuous UV irradiation.

Typically, for R6G, CdSe/ZnS QDs and C-dots, their fluorescence is strong in the beginning but gradually quenches as irradiation time increases to 60 min, 180 min and 10 h of UV irradiation, respectively. In comparison, the SiNSs maintain stable and distinct blue fluorescence, preserving ~80% of the initial intensity after 12-h treatment.

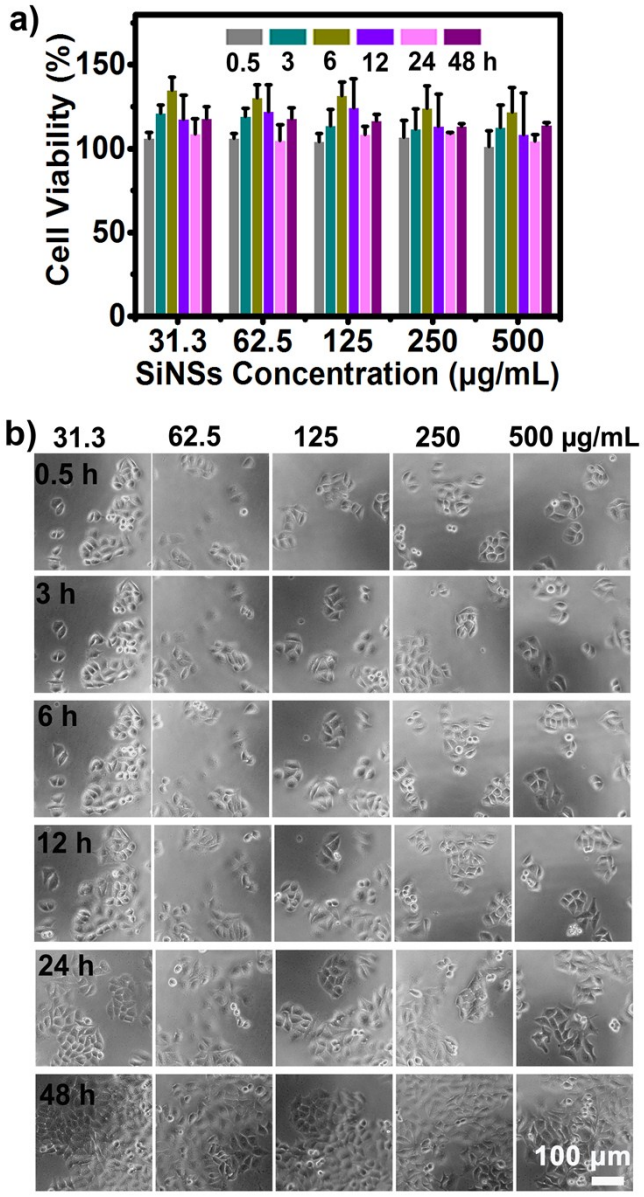

Figure S8. (a) Cell viability of HeLa cells treated with the SiNSs for different incubation time. (b) Morphology of cells incubated with SiNSs of different concentrations (31.3, 62.5, 125, 250 and 500 μg/mL) for 0.5 to 48 h, respectively.

Figure S8 (a) exhibits that the cell viability of HeLa cells treated by the SiNSs preserves >90% at different concentrations (31.3-500 μg/mL) and incubation times (0.5-48 h). Figure S8 (b) shows that the silicon ink-treated HeLa cells maintain normal morphology during 48-h incubation, suggesting negligible cytotoxicity of the resultant SiNSs.

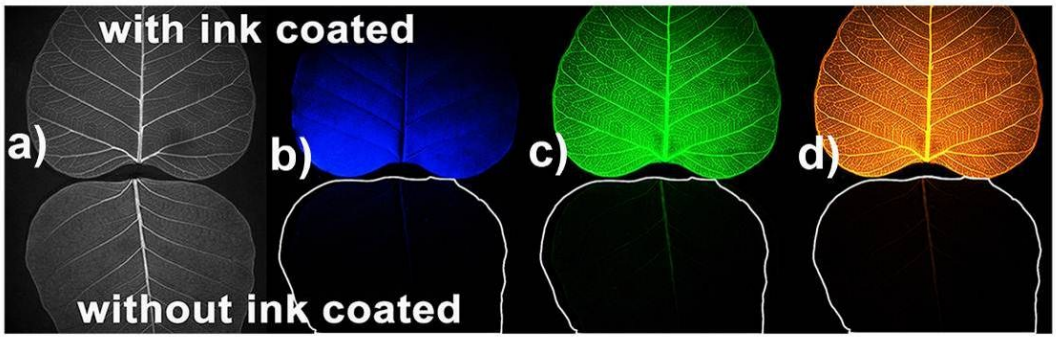

Figure S9. (a) Optical and (b-d) fluorescent images of leaf veins stained with the ink captured by the CRI Maestro in vivo imaging system. (b) excitation at 365 nm, emission at 465-490 nm, and exposure time 1000 ms, (c) excitation at 455 nm, emission at 490-530 nm, and exposure time 1000 ms, and (d) excitation at 523 nm, emission at 550-590 nm, and exposure time 1000 ms. We soak the leaf veins in the solution of SiNSs and then dried under ambient conditions. When the leaf veins are coated with the aqueous solution of SiNSs ink, clear fluorescence is observed in the leaf veins under UV, blue and green light excitation, whereas the leaf veins without the SiNSs ink treatment exhibit negligible fluorescence under the same conditions.

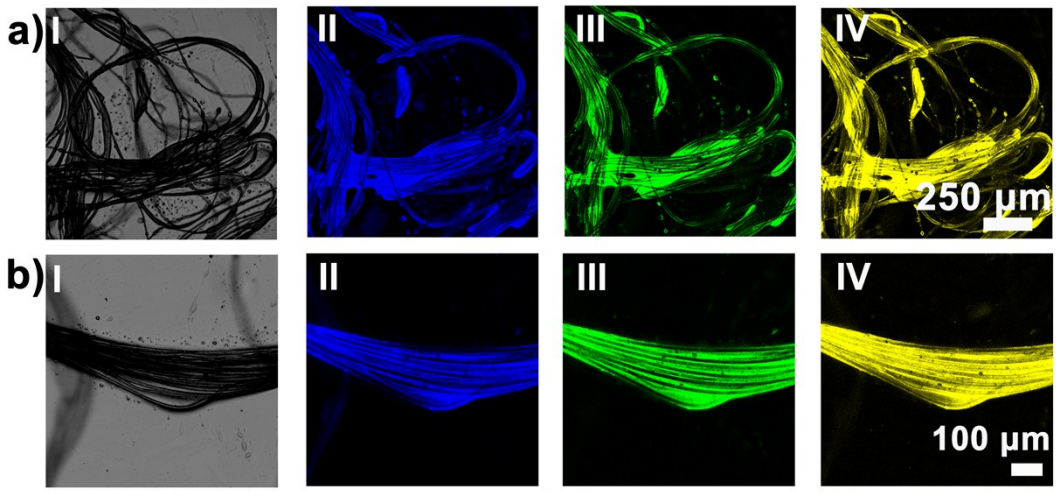

Figure S10. Fluorescent images of synthetic fibers (e.g., Dacron) coated with SiNSs ink (a): (II) λ_{ex} = 405 nm; emission band pass: 430-480 nm; (III) λ_{ex} = 458 nm; emission band pass: 470-550 nm; (IV) λ_{ex} = 514 nm; emission band pass: 560-620 nm. Their corresponding bright-field images are shown in (I). All the pictures are imaged with a LSCM.

The ink-treated fibers could exhibit distinct blue, green and yellow colors upon excitation at 405, 458 and 514 nm, respectively. When the fibers are coated with ink and then dried under air, spectrally resolved fluorescent signals are observed.

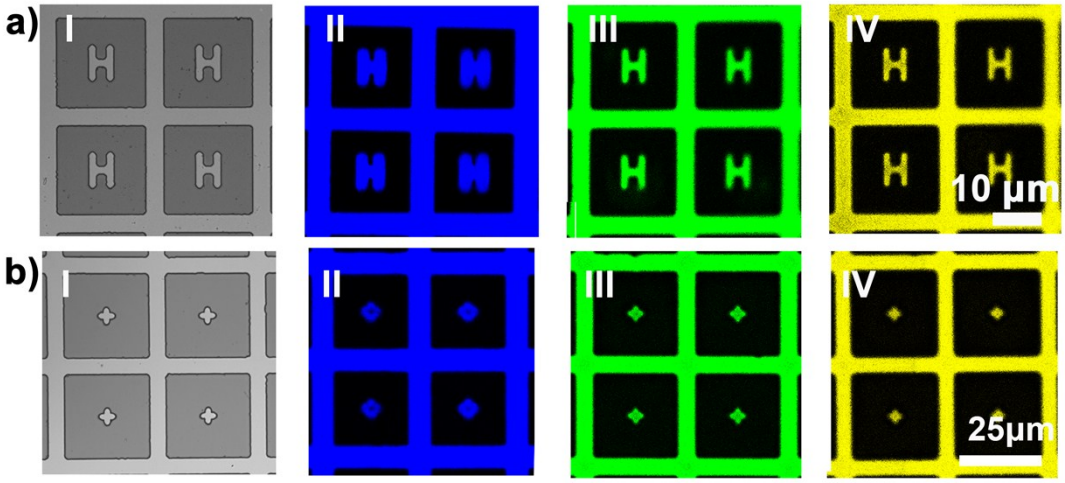

Figure S11. Fluorescent images of hydrophilic photolithography patterns coated with SiNSs ink: (II) λ_{ex} = 405 nm; emission band pass: 430-480 nm; (III) λ_{ex} = 458 nm; emission band pass: 470-550 nm; (IV) λ_{ex} = 514 nm; emission band pass: 560-620 nm. Their corresponding bright-field images are shown in (I). All the pictures are imaged with a LSCM.

The silicon nanoshuttles-based ink, served as a novel kind of fluorescent ink, is also applicable for microcosmic anti-counterfeiting. Specifically, the ink can spread onto hydrophilic patterns prepared by photolithography technology. The SiNSs ink produces visible symbol “H” and “+” emitting blue, green and yellow fluorescence on the hydrophilic patterns, which are respectively detectable under 405, 458 and 514 nm excitation.

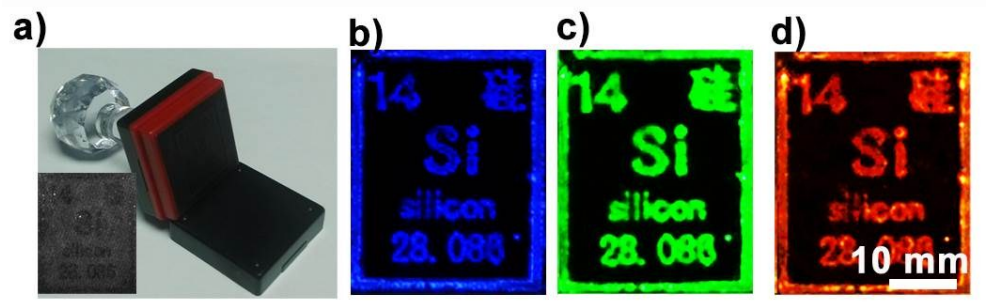

Figure S12. Optical (a) and fluorescent images of the stamper stained with the SiNSs ink captured by the CRI Maestro in vivo imaging system. Excitation at 365 nm, emission at 465-490 nm (b), excitation at 455 nm, emission at 490-530 nm (c), and excitation at 523 nm, emission at 550-590 nm (d). In addition, by utilizing stamper as a model, we further testify feasibility of macroscopic anti-counterfeiting using the fluorescent SiNSs ink. As shown in Figure S12, the SiNSs ink produces visible words "Si silicon" and numbers "28.086" emitting blue, green and yellow fluorescence on the commercially available paper, which is respectively detectable under 365, 455 and 523 nm excitation, indicating important implications for the use of such ink on a macro-scale with multiple colors under different excitation.

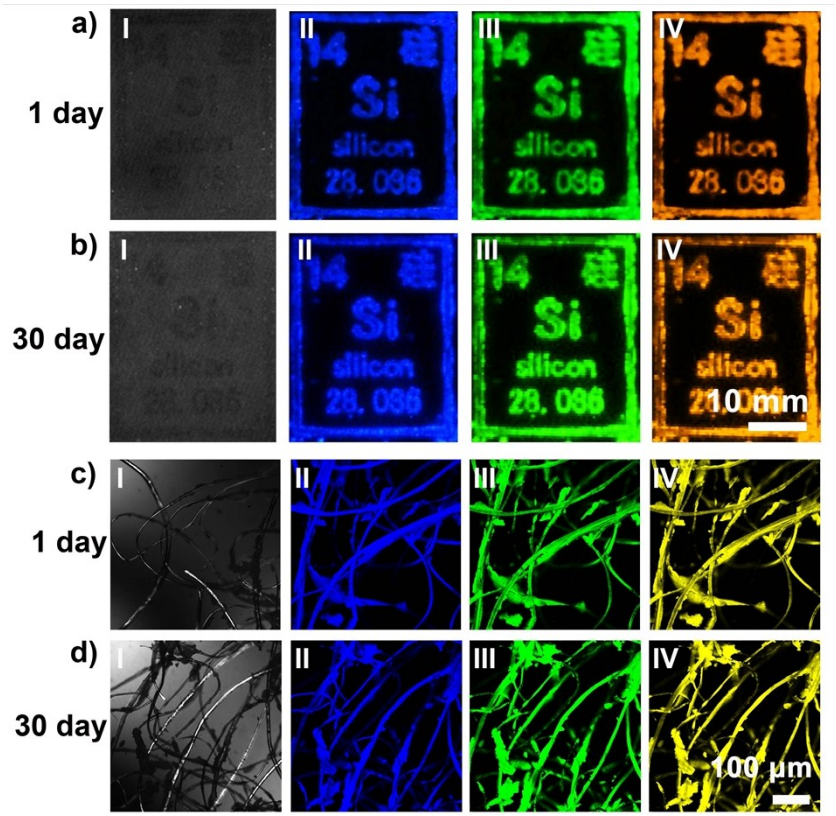

Figure S13. Optical and fluorescent images of paper (a, b) and synthetic fibers (c, d) stained with the SiNSs ink before (a, c) and after (b, d) 30 day storage.

Remarkably, as shown in Figure S13, the SiNSs inks possess excellent physical stability, maintaining bright and stable fluorescence on paper and fibers after over 1 month storage in the ambient environment with no protection

References

(1) (a) B. Song, Y. Zhong, H. Wang, Y. Su, Y. He, *Chem. Commun.,* 2017, **53**, 6957-6960; (b) Y. L. Zhong, F. Peng, F. Bao, S. Y. Wang, X. Y. Ji, L. Yang, Y. Y. Su, S. T. Lee, Y. He, *J. Am. Chem. Soc.,* 2013, **135**, 8350-8356; (c) J. Wang, F. Peng, Y. M. Lu, Y. L. Zhong, S. Y. Wang, M. F. Xu, X. Y. Ji, Y. Y. Su, L. S. Liao, Y. He, *Adv. Optical Mater.,* 2015, **3**, 103-111; (d) T. Yamashita, P. Hayes, *Appl. Surf. Sci.,* 2008, **254**, 2441-2449.

(2) B. Song, Y. Zhong, S. Wu, B. Chu, Y. Su, Y. He, *J. Am. Chem. Soc.,* 2016, **138**, 4824-4831.

(3) (a) M. A. Islam, T. K. Purkait, M. H. Mobarok, I. M. D. Hoehlein, R. Sinelnikov, M. Iqbal, D. Azulay, I. Balberg, O. Millo, B. Rieger, J. G. C. Veinot, *Angew. Chem. Int. Ed.,* 2016, **55**, 7393-7397. (b) C. Guo, Q. Peng, Q. Liu, G. Jiang, *J. Mol. Catal. A: Chem.,* 2003, **192**, 295-302.

(4) (a) Z. Y. Zhang, Y. S. Wu, K. C. Tang, C. L. Chen, J. W. Ho, J. H. Su, H. Tian, P. T. Chou, *J. Am. Chem. Soc.,* 2015, **137**, 8509-8520; (b) S. J. Zhu, Q. N. Meng, L. Wang, J. H. Zhang, Y. B. Song, H. Jin, K. Zhang, H. C. Sun, H. Y. Wang, B. Yang, *Angew. Chem. Int. Ed.,* 2013, **52**, 3953-3957.

(5) (a) K. Sato, S. Yokosuka, Y. Takigami, K. Hirakuri, K. Fujioka, Y. Manome, H. Sukegawa, H. Iwai, N. Fukata, *J. Am. Chem. Soc.,* 2011, **133**, 18626-18633; (b) H. Kim, M. Achermann, L. P. Balet, J. A. Hollingsworth, V. I. Klimov. *J. Am. Chem. Soc.,* 2005, **127**, 544-546; (c) W. D. A. M. De Boer, D. Timmerman, K. Dohnalova, I. N. Yassievich, H. Zhang, W. J. Buma, T. Gregorkiewicz, *Nat. Nanotechnol.,* 2010, **5**, 878-884.